# Supporting Information

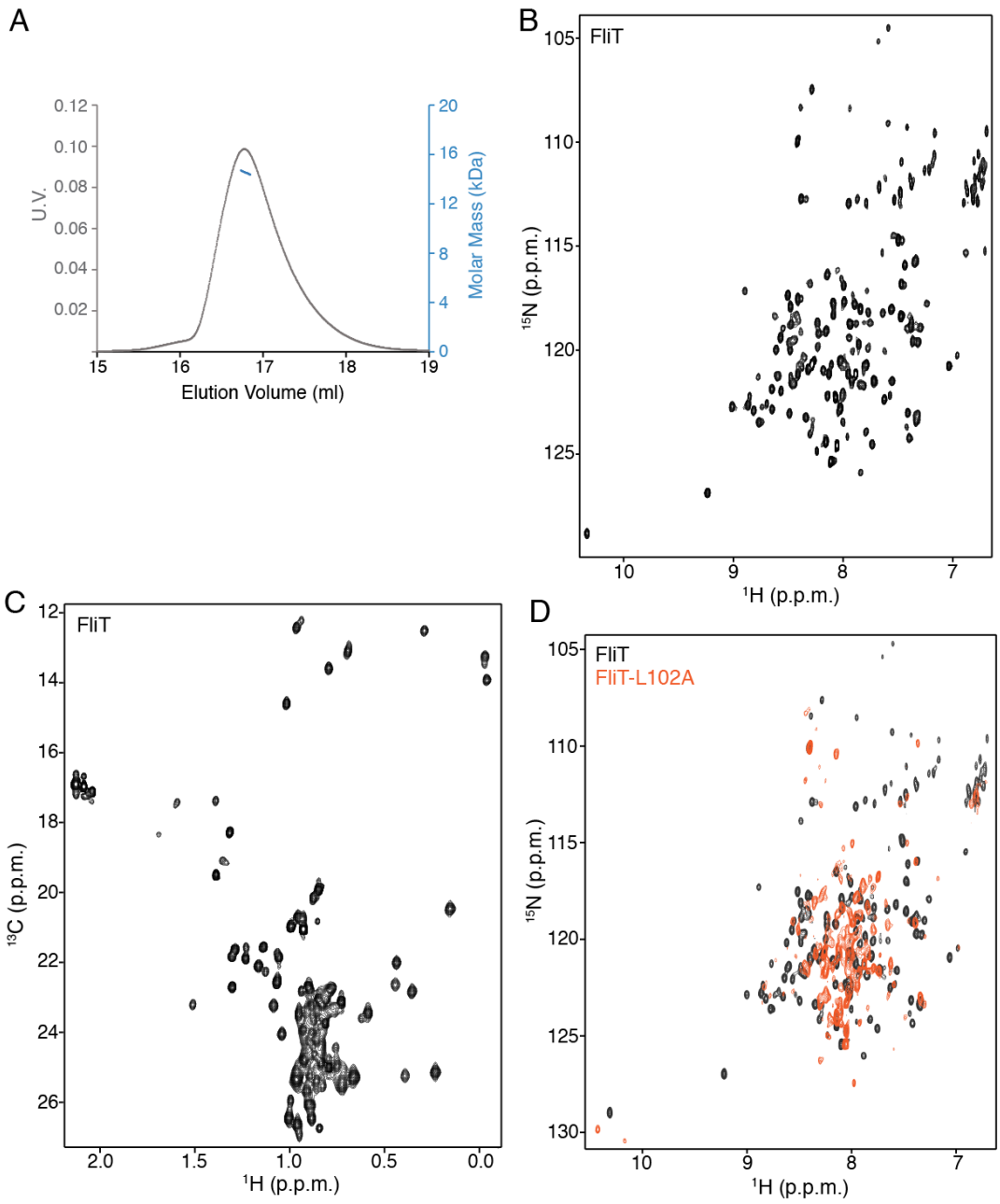



**Fig. S1.** NMR studies of FliT. (A) MALS of FliT shows that the protein exists as a monomer in solution. (B) $^{1}$H-$^{15}$N HSQC and (C) $^{1}$H-$^{13}$C HMQC spectra of U-$^{2}$H,$^{15}$N Ala-$^{13}CH_3$, Met-$^{13}CH_3$, Ile-δ1-$^{13}CH_3$, Leu,Val-$^{13}CH_3$/$^{13}CH_3$, Thr-$^{13}CH_3$. (D) $^{1}$H-$^{15}$N HSQC spectrum of FliT-L102A (orange), superimposed on the spectrum of wild type FliT (black).

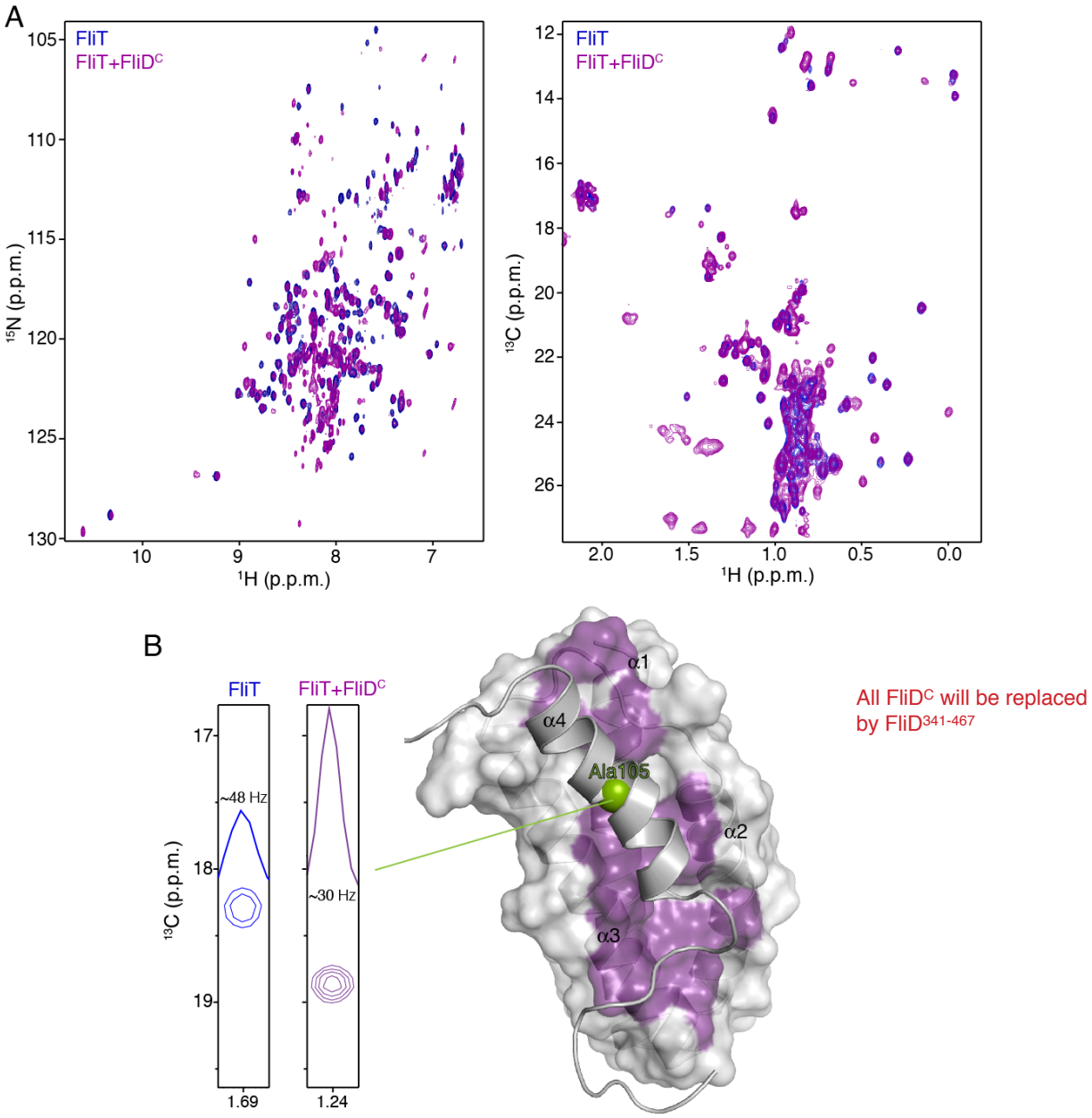



**Fig. S2.** NMR studies of FliD$^{341-467}$ binding to FliT. (A) $^{1}$H-$^{15}$N HSQC (left) and $^{1}$H-$^{13}$C HMQC (right) spectra of U-$^{2}$H,$^{15}$N Ala-$^{13}CH_3$, Met-$^{13}CH_3$, Ile-δ1-$^{13}CH_3$, Leu,Val-$^{13}CH_3$/$^{13}CH_3$, Thr-$^{13}CH_3$ of free FliT (blue) and in complex with FliD$^{341-467}$ (purple). FliT is in excess to ensure that all FliD$^{341-467}$, which has a tendency to aggregate (N-terminal 42 residues/C-terminal 51 residues of FliD are readily degradable. Probably this is the reason we couldn't reach the saturation point), is bound to FliT. (B) NMR analysis shows that FliD$^{341-467}$ binds to the hydrophobic surface formed by FliT helices a1-a3 (purple surface) and helix α4 is displaced. The enhanced mobility of helix α4 in the complex was confirmed by analysis of the linewidth of the helix α4 residues (Ala105 is shown here).

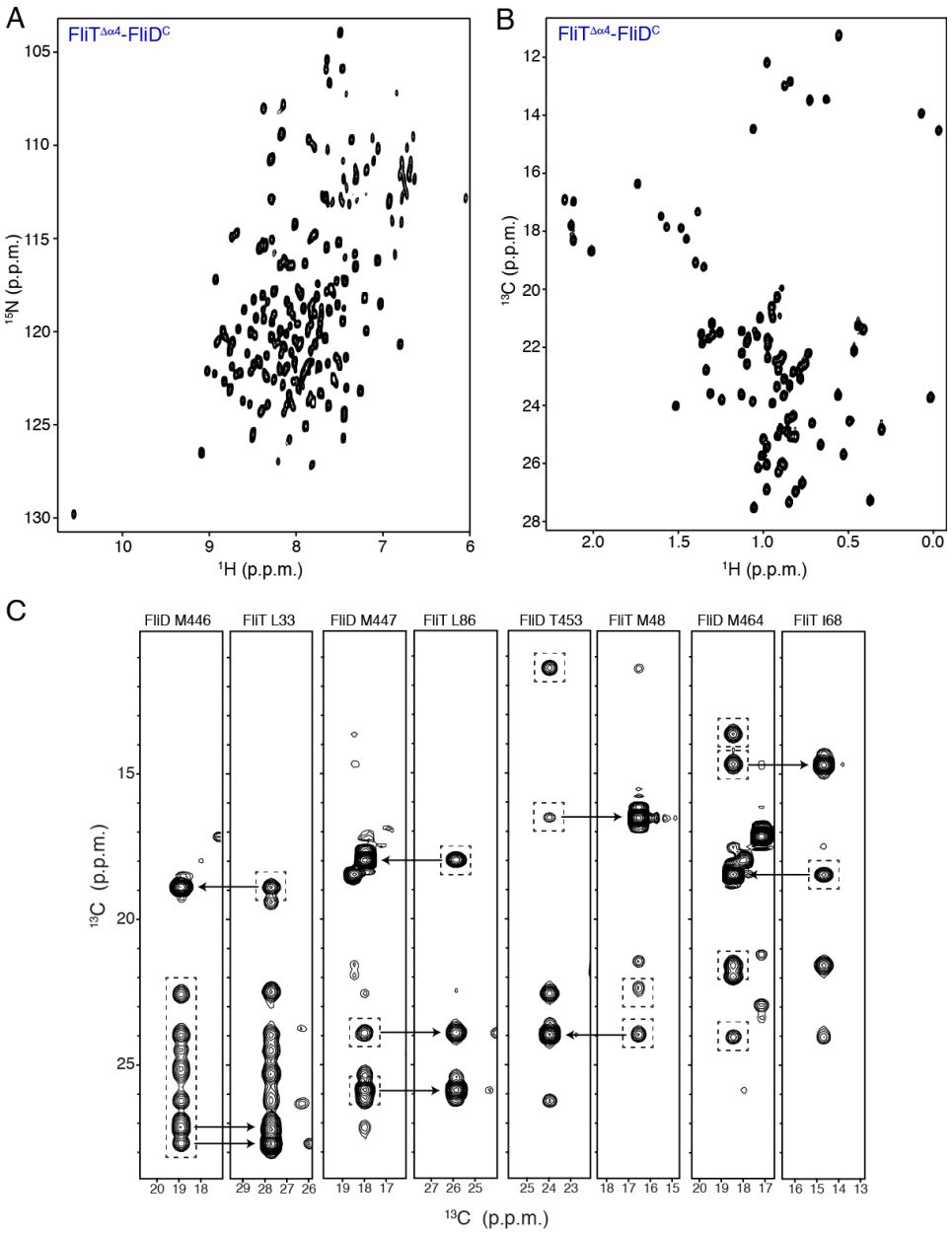



**Fig. S3.** (A) $^{1}$H-$^{15}$N HSQC and (B) $^{1}$H-$^{13}$C HMQC spectra of U-$^{2}$H,$^{15}$N Ala-$^{13}CH_3$, Met-$^{13}CH_3$, Ile-δ1-$^{13}CH_3$, Leu,Val-$^{13}CH_3$/$^{13}CH_3$, Thr-$^{13}CH_3$ of the FliT$^{\Delta\alpha4}$–FliD$^{C}$ complex. (C) Representative NOESY strips showing inter-molecular NOEs between FliT$^{\Delta\alpha4}$ and FliD$^{C}$.

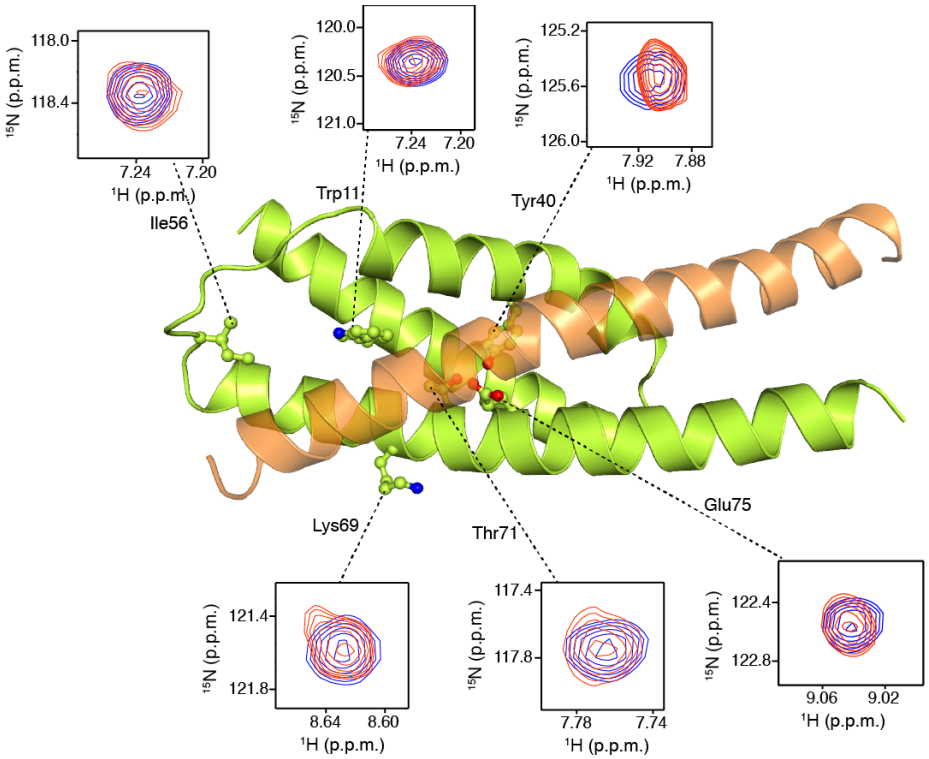



**Fig. S4.** NMR analysis demonstrates that the protein interface in the FliT−FliD$^{C}$ and FliT$^{\Delta\alpha4}$−FliD$^{C}$ complexes is essentially identical. Cross-peaks from $^{1}$H-$^{15}$N HSQC spectra of FliT−FliD$^{341\text{-}467}$ (red) and FliT$^{\Delta\alpha4}$−FliD$^{C}$ (blue) complexes show excellent correspondence.(FliD$^{341\text{-}467}$ was used for titration)

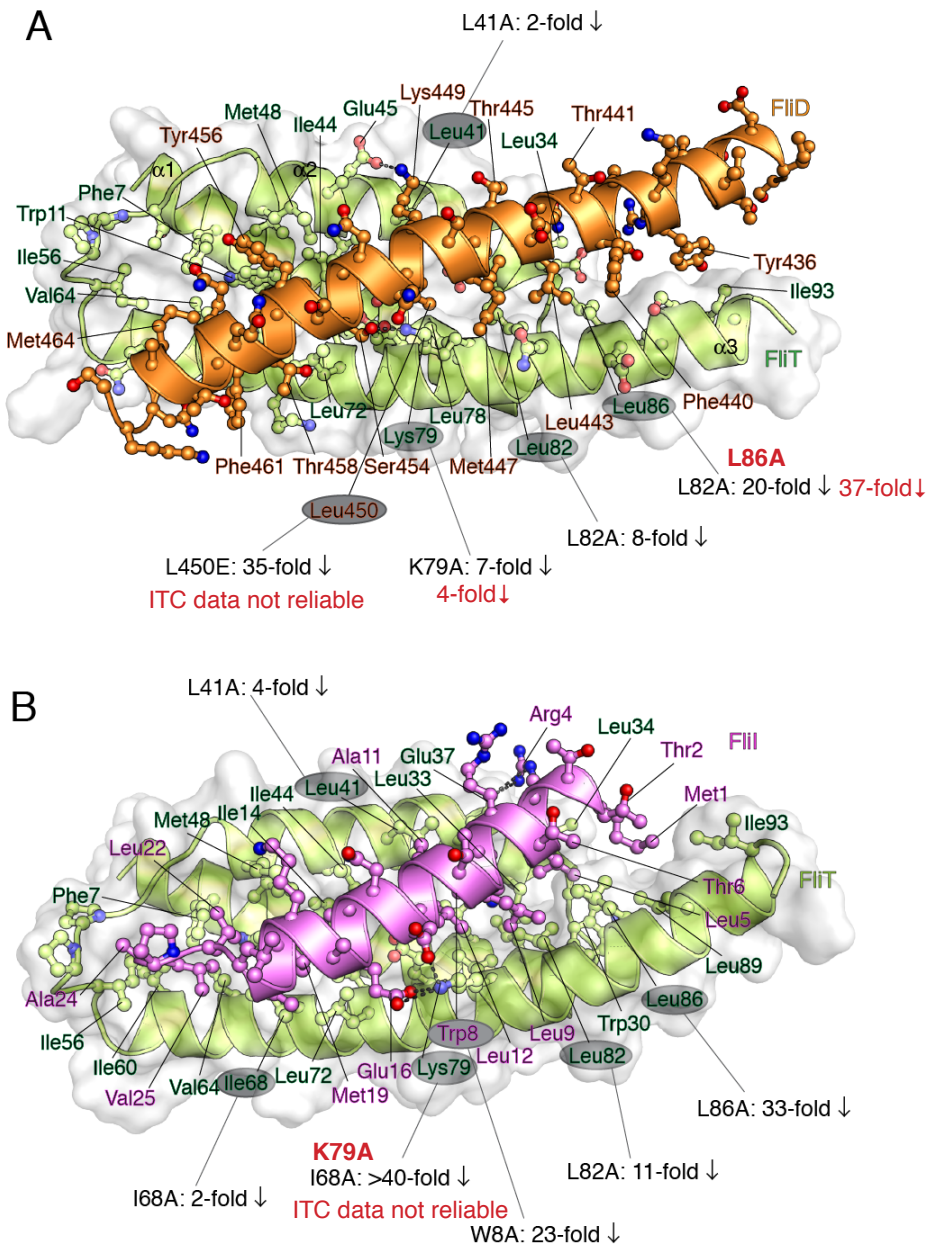



**Fig. S5.** Effect of mutations at the protein interface and their effect on the affinity for the (A) FliT-FliD and (B) FliT-FliI complex. The residues mutated are labeled and the decrease in the measured affinity is indicated. All affinities were measured by ITC.

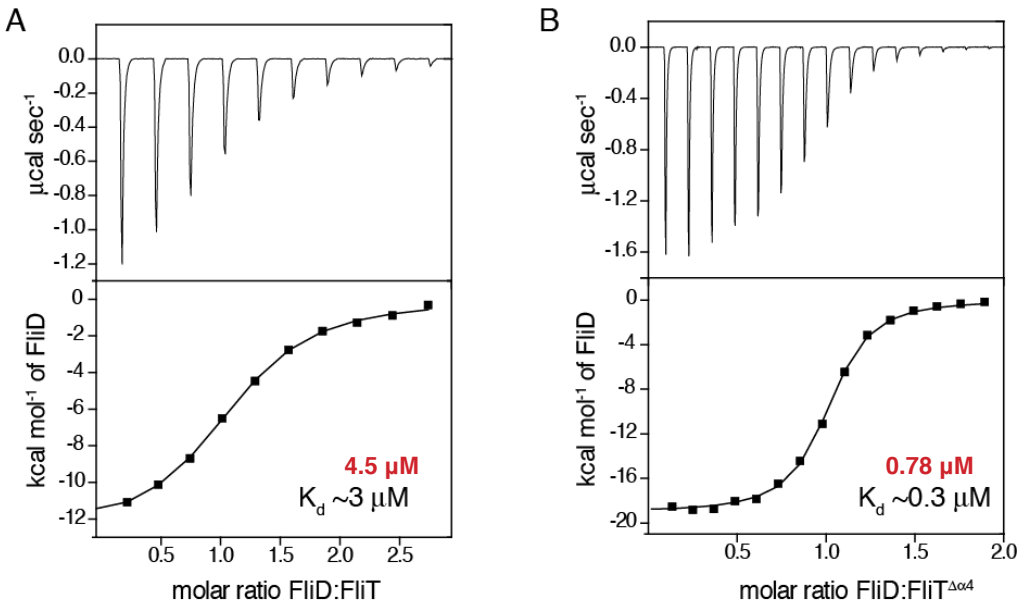



**Fig. S6.** ITC profiles of FliD$^{341\text{-}467}$ binding to (A) FliT and (B) FliT$^{\Delta\alpha4}$. FliD$^{341\text{-}467}$ binds with a 6-fold higher affinity to FliT$^{\Delta\alpha4}$ wherein autoinhibition is relieved .

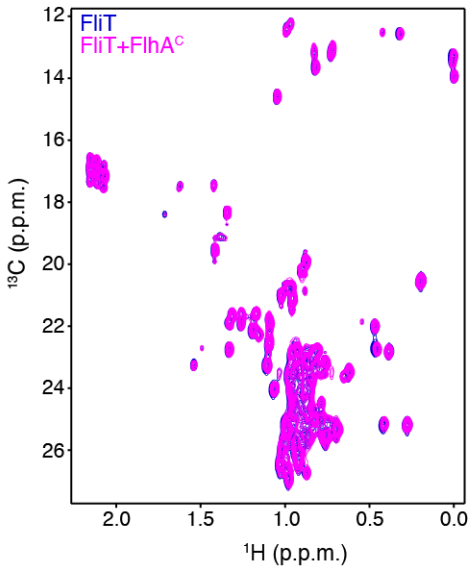



**Fig. S7.** $^{1}$H-$^{13}$C HMQC spectra of U-$^{2}$H,$^{15}$N Ala-$^{13}CH_3$, Met-$^{13}CH_3$, Ile-δ1-$^{13}CH_3$, Leu,Val-$^{13}CH_3$/$^{13}CH_3$, Thr-$^{13}CH_3$ of free FliT (blue) and in the presence of FlhA$^{C}$ (magenta) show that free FliT does not interact with FlhA$^{C}$. $^{15}$N HSQC titration shows weak interaction between FliT and FlhA$^{C}$.

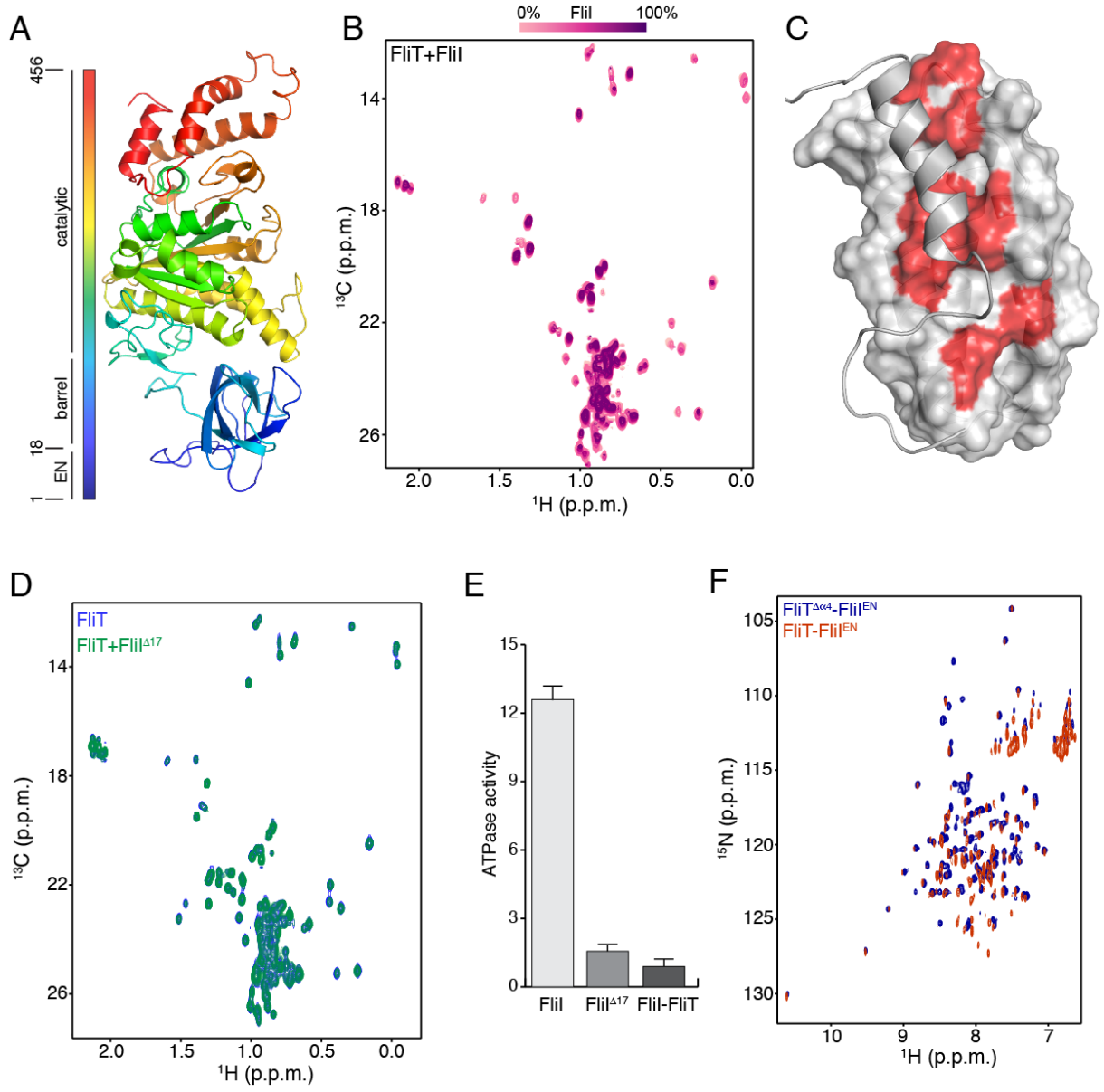



**Fig. S8.** Interaction between FliT and FliI. (A) Structure of FliI (PDB ID 2DPY). The extreme N terminal region was not crystallographically resolved and it was modeled here as an unstructured region. (B) Stepwise titration of unlabeled FliI to U-$^{2}$H,$^{15}$N Ala-$^{13}CH_3$, Met-$^{13}CH_3$, Ile-δ1-$^{13}CH_3$, Leu,Val-$^{13}CH_3$/$^{13}CH_3$ labeled FliT. (C) The FliT residues affected by FliI binding are colored red on the FliT surface. (D) NMR spectra show that the FliI$^{\Delta 17}$ variant does not bind to FliT. (E) ATPase activity of FliI, FliI$^{\Delta 17}$ and FliI in complex with FliT. (Unit of ATPase activity = nmoles of hydrolyzed ATP/µg of protein , FliI = 5.06 nmoles/µg, FliI$^{\Delta 17}$ = 0.026 nmoles/µg, FliI-FliT = 0.55 nmoles/µg) (F) $^{1}$H-$^{15}$N HSQC spectra of FliT−FliI$^{EN}$ (orange) and FliT$^{\Delta\alpha 4}$−FliI$^{EN}$ (blue) complexes show very similar chemical shifts.

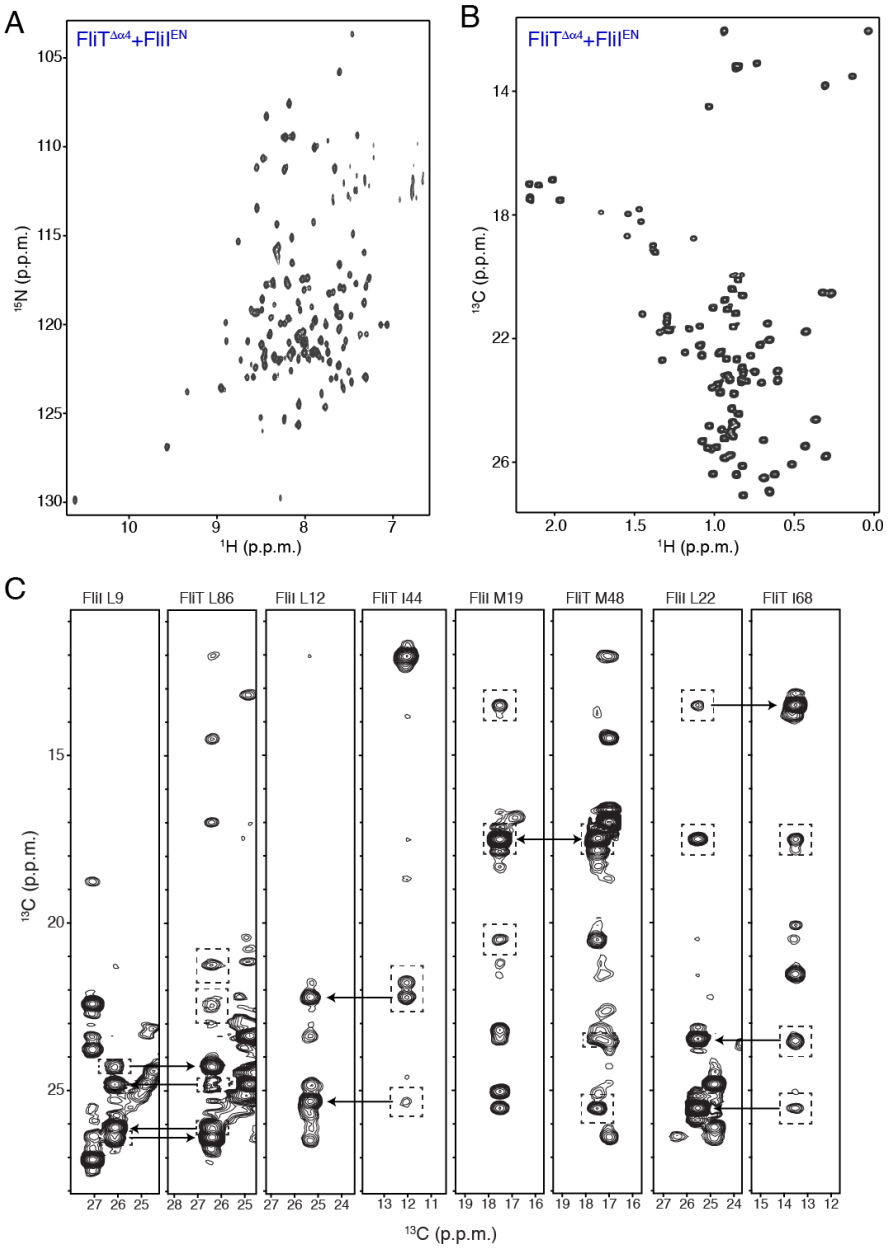



**Fig. S9.** (A) $^{1}$H-$^{15}$N HSQC and (B) $^{1}$H-$^{13}$C HMQC spectra of U-$^{2}$H,$^{15}$N Ala-$^{13}$CH$_3$, Met-$^{13}$CH$_3$, Ile-δ1-$^{13}$CH$_3$, Leu,Val-$^{13}$CH$_3$/$^{13}$CH$_3$, Thr-$^{13}$CH$_3$ of the FliT$^{\Delta\alpha4}$–FliI$^{EN}$ complex. (C) Representative NOESY strips showing inter-molecular NOEs between FliT$^{\Delta\alpha4}$ and FliI$^{EN}$.

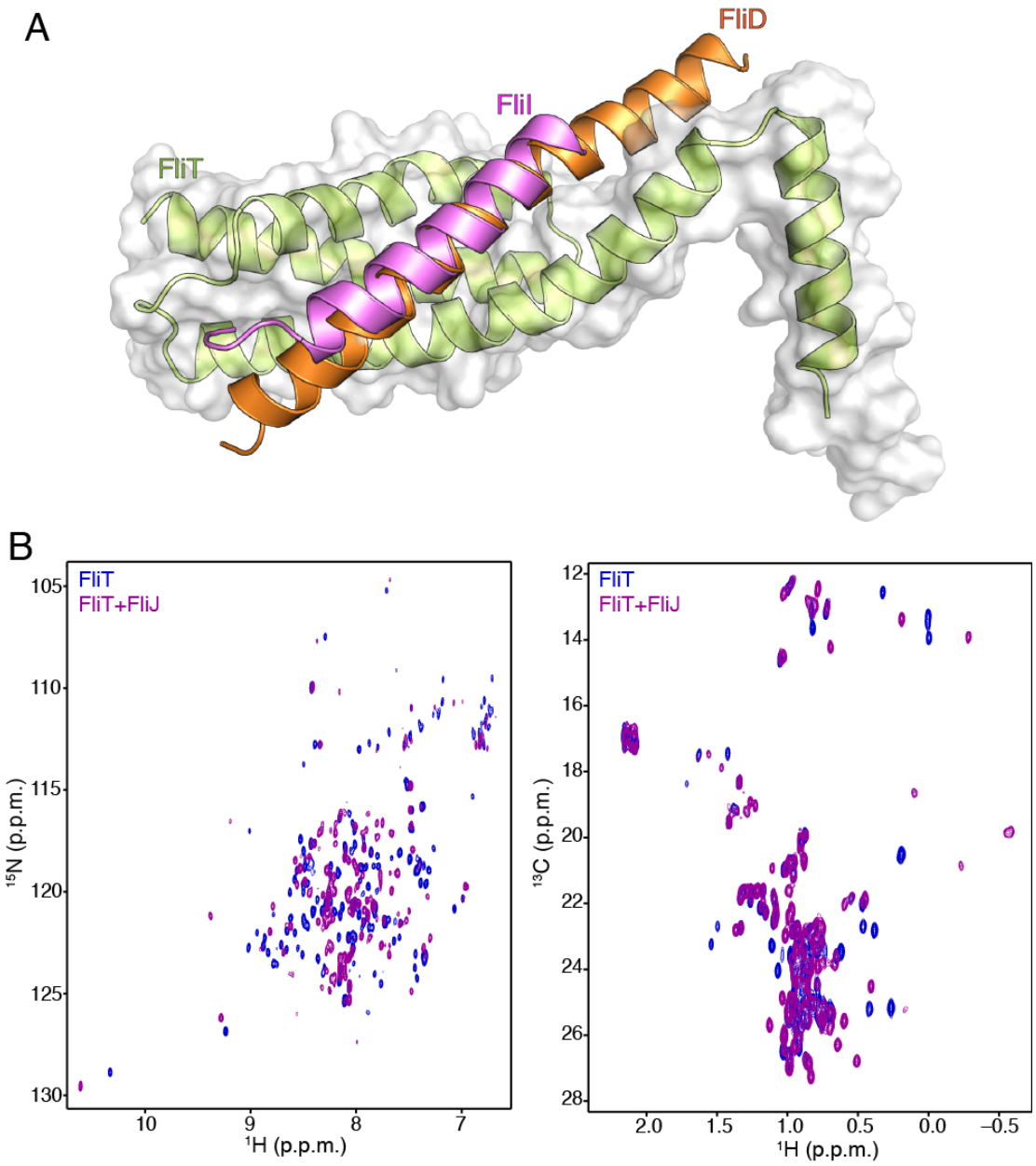



**Fig. S10.** (A) Superposition of the FliT−FliI$^{EN}$ and FliT−FliD$^{C}$ structures demonstrates that FliI and FliD bind to the same surface on FliT. (B) $^{1}$H-$^{15}$N HSQC (left) and $^{1}$H-$^{13}$C HMQC (right) spectra of U-$^{2}$H,$^{15}$N Ala-$^{13}CH_3$, Met-$^{13}CH_3$, Ile-δ1-$^{13}CH_3$, Leu,Val-$^{13}CH_3$/$^{13}CH_3$, Thr-$^{13}CH_3$ of free FliT (blue) and in complex with FliJ (purple). NMR analysis shows that FliJ binds to the same surface on FliT as FliD and FliI do.